RSC Advances

PAPER

View Article Online
View Journal | View Issue



Cite this: *RSC Adv.*, 2017, **7**, 15084

# Bright green emission from f-MWCNT embedded co-doped $Bi^{3+}$ + $Tb^{3+}$:polyvinyl alcohol polymer nanocomposites for photonic applications

K. Naveen Kumar,*[a] R. Padma,[b] Y. C. Ratnakaram[b] and Misook Kang*[a]

Received 23rd January 2017
Accepted 20th February 2017

DOI: 10.1039/c7ra01007a

rsc.li/rsc-advances

A bright, dazzling green emission has been obtained from functionalized multi walled carbon nanotube (f-MWCNTs)-embedded $Bi^{3+}$ + $Tb^{3+}$:PVA polymer nanocomposites under UV excitation. We successfully synthesized $Tb^{3+}$:PVA, $Bi^{3+}$ + $Tb^{3+}$:PVA and $Bi^{3+}$ + $Tb^{3+}$ + f-MWCNTs:PVA polymer films by a solution casting method. For these polymer films, their XRD and FTIR spectral profiles were analyzed for structural details and ion–polymer interaction mechanism. $Tb^{3+}$ doped at different concentrations in PVA polymer films displayed a green emission at 546 nm ($^5D_4 \rightarrow {}^7F_5$) under 370 nm ($^7F_6 \rightarrow {}^5L_{10}$) excitation. Upon co-doping with $Bi^{3+}$ in the $Tb^{3+}$:PVA polymer film, the film exhibits enriched green emission compared to single $Tb^{3+}$:PVA under 320 nm excitation due to the energy transfer from $Bi^{3+}$ to $Tb^{3+}$. Surprisingly, a common excitation band was found at 320 nm for $Tb^{3+}$, $Bi^{3+}$ and f-MWCNTs. After dispersion of the f-MWCNTs in the co-doped $Bi^{3+}$+$Tb^{3+}$:PVA polymer films, the photoluminescence properties were remarkably enhanced, and a prominent green emission was observed at 546 nm. The green emission of $Tb^{3+}$ is significantly enhanced though an efficient energy transfer process from $Bi^{3+}$ to $Tb^{3+}$ and f-MWCNTs to $Tb^{3+}$. The possible energy transfer mechanism was clearly demonstrated *via* several fluorescent methods. The energy transfer mechanism was substantiated with fluorescence lifetime decay dynamics. From these results, these f-MWCNTs-embedded $Bi^{3+}$+$Tb^{3+}$:PVA polymer films could be suggested as promising candidates for green luminescent materials for photonic devices.

## 1. Introduction

In recent years, trivalent rare earth ion-doped organic luminescent materials have gained abundant interest in their processing for their use in the field of photonics, such as display devices, optical sensors and light emitting diodes (LEDs). Much attention has been focused on these promising materials that consist of lanthanide–organic frameworks because of the intrinsic physical properties of the trivalent lanthanide ions.[1] Rare earth doped complexes are widely used in several photonic devices because of their superior advantages such as narrow emission bands for high color purity, long lifetime, large stokes shifts, high quantum efficiency and good processability. These versatile materials could also be considered as light converting molecular devices (LCMD).[2] Nevertheless, rare earth–organic complexes are found to be potential candidates for luminescence and electroluminescence devices, detector optical displays, telecommunications, optical signal displays, energy-harvesting devices and for use in a variety of areas such as fluoroimmunoassay.[3] Polymer-rare earth complexes have more advantages such as light weight, ease of fabrication, design flexibility and excellent mechanical properties and transparency over other inorganic complexes.[4] Polyvinyl alcohol (PVA) exhibits semicrystallinity and has several advantages such as solubility in water, chemical resistance, high mechanical strength, good processability, good charge storage capacity and high dielectric strengths over other polymers. PVA is widely used in the fields of contact lenses, synthetic fibers, papers, textile, coatings and binding industry.[5] Because of the electronic transitions between the 4f orbitals, the rare earth ions exhibit prominent luminescence characteristics. The emission transitions yield sharp spectral lines in the optical spectra because the $4f^n$ shells are shielded by the $5S^2$ and $5P^6$ orbitals. Specifically, some lanthanide ions, such as $Sm^{3+}$, $Dy^{3+}$, $Eu^{3+}$ and $Tb^{3+}$, can emit a characteristic fluorescence with a high photoluminescence efficiency and long fluorescence lifetime due to the f–f transition. Terbium ($Tb^{3+}$) has unique properties over the other rare earth ions. It shows an intense green emission at 546 nm due to the $^5D_4 \rightarrow {}^7F_5$ electronic transition. $Tb^{3+}$ consists of broad excitation bands in the short and long wavelength regions due to $4f^8 \rightarrow 4f^7\ 5d^1$ and $4f^8 \rightarrow 4f^8$ electronic transitions, respectively. Hence, if any sensitizer ion possessing strong absorption or excitation in the UV region is situated near $Tb^{3+}$ ions in a complex, they can easily enhance the $Tb^{3+}$ emission through energy transfer process (sensitizer for $Tb^{3+}$

[a]*Department of Chemistry, College of Science, Yeungnam University, Gyeongsan, Gyeongbuk 38541, Republic of Korea. E-mail: knaveenphy@gmail.com; mskang@ynu.ac.kr*

[b]*Department of Physics, Sri Venkateswara University, Tirupati-517502, A.P., India*

ions).[6] In this perspective, $Bi^{3+}$ has been co-doped with $Tb^{3+}$ to enhance the $Tb^{3+}$ ion emission performances because $Bi^{3+}$ exhibits strong excitation in the UV region due to the $^1S_0 \rightarrow {}^3P_0$ transition. It can activate $Tb^{3+}$ ions efficiently as a sensitizer to obtain the intense green emission.[7] In spite of the addition of $Bi^{3+}$ ions to the $Tb^{3+}$ ion doped complexes, the green emission of the $Tb^{3+}$ ions has been reduced, probably due to a concentration quenching effect above the optimized concentration of $Bi^{3+}$ ions. The luminescence quenching occurs due to ionic aggregation, and this aggregation acts as a quenching center.[8] To overcome this situation, we can choose another strategy, which is the addition of a suitable nanofiller, to obtain further luminescence efficiency from the activator ion.[9] Homogeneous dispersions of nanofiller in the polymer matrix could become a new field of research for several advanced applications. Much research effort has been made to obtain an improvement in the luminescence efficiency while retaining the mechanical properties and stability towards metallic anodes by the incorporation of nanofillers.[10] Nevertheless, by encapsulating the MWCNTs in the rare earth complexes like phosphors and nanostructures, the photoluminescence properties of the rare earth ions are drastically decreased.[11] However, in some cases, the MWCNT assembled rare earth complexes show prominent photoluminescence features under long UV exposure. This might be due to the relatively rigid environment of the MWCNTs. Moreover, the MWCNTs can protect the complexes from decomposing under UV irradiation.[12] Based on this unique character of the MWCNTs, we made an attempt to incorporate the f-MWCNTs into a terbium-doped PVA polymer complex. In our present study, f-MWCNTs were dispersed in co-doped $Bi^{3+}$+$Tb^{3+}$:PVA polymer films at different concentrations to obtain enhanced emission intensities of $Tb^{3+}$.

## 2. Experimental

### 2.1 Functionalization process of MWCNTs

The raw material of the MWCNTs was refluxed in an $H_2SO_4$–$HNO_3$ mixture in a 3 : 1 (v/v) ratio for 20 h. The obtained mixture was filtered properly after dilution. In order to remove the traces of solvents and excess acid from this solution, we washed the mixture several times under vacuum with DD water. The obtained material was kept at 110 °C for 12 h in an oven. The final product was crushed and properly ground with a cleaned mortar to get f-MWCNT powder.[13]

### 2.2 Preparation of MWCNT embedded $Bi^{3+}$ + $Tb^{3+}$:PVA polymer nanocomposite films

$Bi^{3+}$ and $Tb^{3+}$ ion doped polymer composite films were prepared by employing a solution casting method. Standard chemicals of polyvinyl alcohol (PVA) (MW = $186 \times 10^3$), bismuth nitrate pentahydrate [$Bi(NO_3)_3 \cdot 5H_2O$], terbium nitrate pentahydrate [$Tb(NO_3)_3 \cdot 5H_2O$] and multiwalled carbon nanotubes (MWCNTs) were purchased from Sigma-Aldrich. Precursor chemicals were taken in appropriate weight percentage ratios using triple distilled water as a solvent. Initially, PVA and the dopant salts were properly dissolved in triple distilled water in one beaker. The functionalized MWCNTs were dispersed in water at various concentrations (0.01, 0.02, 0.03, 0.04, 0.05, 0.06 and 0.07 mg) in a separate beaker using an ultrasonicator. These two solutions were intermixed in another separate beaker and continuously stirred at RT (~30 °C) for 10–12 h until the mixture was homogeneous. The obtained solution was cast onto polypropylene dishes, and those solutions were allowed to evaporate slowly at RT. The final product was dried upon warming to remove all traces of the solvent. The dried f-MWCNT embedded co-doped $Bi^{3+}$ + $Tb^{3+}$:PVA polymer nanocomposite films were collected for further characterization.

## 3. Characterization

X-ray diffraction profiles of the rare earth doped PVA polymer with and without f-MWCNTs were recorded on a SEIFERT 303 TT X-ray diffractometer (XRD) with CuKα (1.5405 Å). It was operated at 40 kV and 50 mA of voltage and anode currents, respectively, at an angle ranging from 10° to 90° and a scan speed of 10° $min^{-1}$. FT-IR spectra of the prepared samples were carried out on EO-SXB IR spectrometer in the range of 4000–500 $cm^{-1}$. Phillips TECHNAI FE 12 transmission electron microscopy (TEM) was used for particle size and shape confirmation and operated at 120 kV. The TG measurements for the pure PVA, $Tb^{3+}$:PVA, $Bi^{3+}$:PVA and $Bi^{3+}$ + $Tb^{3+}$ + f-MWCNTs:PVA polymer films were carried out using thermo-gravimetric analysis and differential scanning calorimetry, Model: SDTQ600TA Instrument (specimens were scanned in the nitrogen atmosphere from 30–60° at a heating rate of 10 °C $min^{-1}$) from RT to 700 °C. The photoluminescence (excitation and emission) spectra of $Tb^{3+}$:PVA, $Bi^{3+}$:PVA films and $Bi^{3+}$ + $Tb^{3+}$ + f-MWCNTs:PVA polymer nanocomposites were recorded on a Scinco FluoroMate FS-2 visible fluorescence spectrometer with a Xe arc lamp of 150 W as an excitation source for a steady state emission spectrum measurement.

## 4. Results and discussion

### 4.1 XRD analysis

X-ray diffractometer data was recorded before functionalization and after functionalization of the MWCNTs and are presented in the insert of Fig. 1(f). The intense diffraction peak at $2\theta$ of 25.2° corresponds to the (002) plane, and the two low intensity peaks at 42.6° and 52.7° corresponds to (100) and (004) planes of the MWCNTs.[14] X-ray diffraction investigations were performed to confirm the microstructural changes that take place as well as to characterize the molecular structure of the various polymer composites. The diffraction patterns of pure PVA, $Tb^{3+}$:PVA, $Bi^{3+}$:PVA, co-doped $Bi^{3+}$ + $Tb^{3+}$:PVA polymer composite films with and without f-MWCNTs are shown in Fig. 1(a)–(e). The un-doped PVA polymer film exhibits an intense diffraction peak at 19.2°, a weak shoulder at 22.3° and a low intensity peak at 40.2°, which correspond to the characteristic reflections of the (101), (200) and (111) planes of the monoclinic unit cell (JCPDS: 53-1587) of PVA, respectively.[15,16] Upon doping $Bi^{3+}$ or $Tb^{3+}$ ions in the PVA polymer matrix, the intensity of the characteristic diffraction peaks decreased. This variation in intensity suggests that the strong interactions between the polymer chains and the dopant ions lead to the

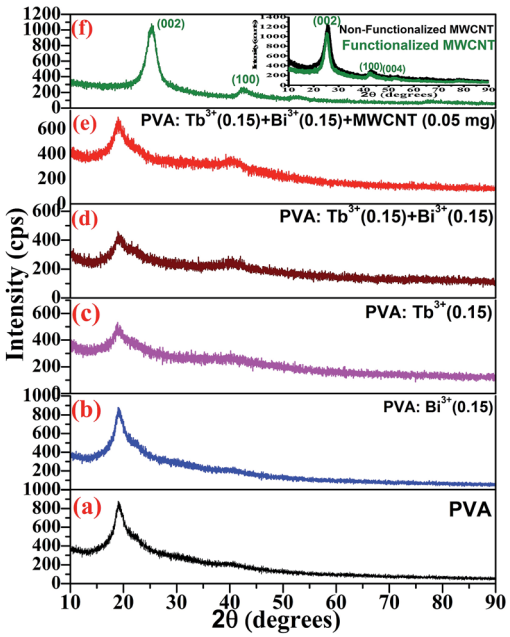


Fig. 1 (a) XRD profiles of pure (a) PVA, (b) $Bi^{3+}$:PVA, (c) $Tb^{3+}$:PVA, (d) ($Bi^{3+}$ + $Tb^{3+}$):PVA, (e) ($Bi^{3+}$ + $Tb^{3+}$) + f-MWCNTs (0.05 mg):PVA polymer films and (f) f-MWCNTs.

disruption of the semicrystalline phase of the PVA bonding scheme.[17] Due to the addition of a very small amount of f-MWCNTs in the co-doped PVA polymer system, the diffraction peaks pertaining to f-MWCNTs were not found.

### 4.2 TEM analysis

The TEM images of the MWCNTs, which are in an agglomerated form and are hydrophobic, are shown in Fig. 2(a). After functionalization, they were separated from each other and possessed a hydrophilic nature, as shown in Fig. 2(b). These functionalized MWCNTs were more convenient agents to disperse in the polymer composites for further investigation. The functionalized MWCNTs were well dispersed in the polymer composite films and are shown in Fig. 2(c). The f-MWCNTs and polymer are clearly represented in Fig. 2(c). In the figure, the black background could be the polymer, and the tube-like structures indicate the f-MWNTs.

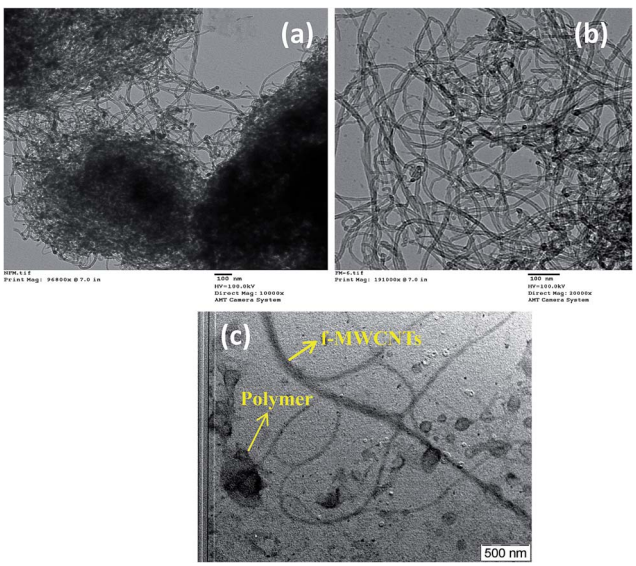


Fig. 2 TEM images of (a) non-functionalized MWCNTs, (b) functionalized MWCNTs, (c) f-MWCNTs (0.05 mg) embedded co-doped $Bi^{3+}$ (0.15 wt%) + $Tb^{3+}$ (0.15 wt%):PVA polymer nanocomposites.

### 4.3 FTIR analysis

Complex formation and intermolecular interaction studies in the solid dispersions were extensively analyzed from the Fourier transform infrared (FTIR) spectroscopy. FTIR spectra of the pure PVA, PVA:$Bi^{3+}$, PVA:$Tb^{3+}$, PVA:$Bi^{3+}$ + $Tb^{3+}$ and f-MWCNT embedded PVA:$Bi^{3+}$ + $Tb^{3+}$ polymer matrix were recorded in the range of 4000–530 $cm^{-1}$, as shown in Fig. 3. We observed a broad peak from 3670–3000 $cm^{-1}$, which centered at 3285 $cm^{-1}$. This was attributed to the symmetric stretching vibrations of the O–H from the intramolecular and intermolecular hydrogen bonds in PVA. The stretching vibrational peak –OH is sensitive to hydrogen bonds in PVA. The bands pertaining to symmetric and anti-symmetric stretching vibrational modes of the C–H alkyl groups were observed at 2848 $cm^{-1}$ and 2919 $cm^{-1}$.[18,19] The band at 1657 $cm^{-1}$ was observed, and it was attributed to the acetyl C=C group in the PVA polymer matrix. We observed two bands at 1581 $cm^{-1}$ and 1436 $cm^{-1}$, which were ascribed to aromatic C=C stretching and $CH_2$ bending vibrations, respectively. The wagging vibrational mode of the $CH_2$ group was observed at 1367 $cm^{-1}$. The combination of the C–H wagging vibrational and C–O stretching of the acetyl groups was observed at 1256 $cm^{-1}$. The band at 1092 $cm^{-1}$ was observed, and it was attributed to the hydroxyl C–O stretching.[19] The most significant bands were observed at 952 $cm^{-1}$ and 836 $cm^{-1}$, and these bands were assigned to the C–C stretching and $CH_2$ stretching vibrations. The band assignments of the FTIR profiles of pure PVA, PVA:$Bi^{3+}$, PVA:$Tb^{3+}$, PVA:$Bi^{3+}$ + $Tb^{3+}$ and f-

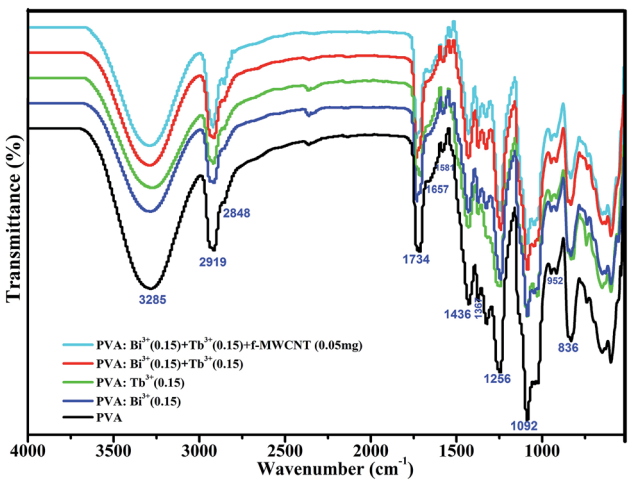


Fig. 3 FTIR profiles of PVA, $Bi^{3+}$:PVA, $Tb^{3+}$:PVA, ($Bi^{3+}$ + $Tb^{3+}$):PVA, and ($Bi^{3+}$ + $Tb^{3+}$) + f-MWCNTs (0.05 mg):PVA polymer films.

Table 1 FTIR bands assignment of the (a) PVA (b) PVA:$Bi^{3+}$ (0.15), (c) PVA:$Tb^{3+}$ (0.15), (d) PVA:$Bi^{3+}$ (0.15) + $Tb^{3+}$ (0.15) and (e) PVA:$Bi^{3+}$ (0.15) + $Tb^{3+}$ (0.15) + f-MWCNTs (0.05 mg)

| | Wavenumber ($cm^{-1}$) | | | | | |
|---|---|---|---|---|---|---|
| Assignment of the bands | *a* | *b* | *c* | *d* | *e* | Ref. |
| OH stretching vibrations | 3285 | 3286 | 3287 | 3389 | 3394 | 18 and 19 |
| CH symmetric stretching | 2848 | 2849 | 2852 | 2857 | 2857 | 18 and 19 |
| CH anti symmetric stretching | 2919 | 2921 | 2921 | 2922 | 2928 | 18 and 19 |
| Acetyl C=C group | 1657 | 1664 | 1670 | 1678 | 1681 | 18 |
| Aromatic C=C stretching group | 1581 | 1584 | 1589 | 1592 | 1598 | 18 |
| $CH_2$ bending vibrations | 1436 | 1438 | 1438 | 1438 | 1440 | 18 |
| $CH_2$ wagging vibration | 1367 | 1367 | 1368 | 1372 | 1374 | 18 |
| C–H wagging mode, C–O stretching of acetyl groups | 1256 | 1257 | 1257 | 1259 | 1259 | 18 |
| Hydroxyl C–O stretching | 1092 | 1093 | 1093 | 1094 | 1094 | 19 |
| C–C stretching vibrational mode | 952 | 954 | 955 | 957 | 959 | 18 |
| $CH_2$ stretching vibration | 836 | 838 | 839 | 842 | 848 | 18 |

MWCNTs embedded PVA:$Bi^{3+}$ + $Tb^{3+}$ polymer matrix are listed in Table 1. Compared with pure PVA, the –OH stretching peak position slightly shifted to a higher wavenumber in the doped PVA polymer system, and a slight intensity change in the C=O stretching peak was observed in the doped PVA polymer matrix, suggesting the presence of hydrogen bonding interactions between the hydroxyl groups on the PVA molecular chains.

Upon doping with $Bi^{3+}$ and $Tb^{3+}$ ions with and without f-MWCNTs, the FTIR spectral profile of the PVA polymer matrix was found to be slightly modified. We observed the variation in the intensity in the FTIR spectra peaks upon doping, and this explores the information regarding the formation of the polymer complex between the pure polymer and dopant ions. The stretching vibrational mode of the carbonyl groups (C=O) was observed at 1734 $cm^{-1}$.

This band could be ascribed to the absorption of hydrogen ions from the OH groups of the main chain of the PVA polymer matrix. Interestingly, the intensity of the C=C band and other bands was found to decrease upon the addition of the rare earth ions, which indicates a decrease in the number of C=C groups along the PVA main chain. This could be attributed to the interaction between the C=C groups and the hydrogen, which was abstracted from the O–H groups of the PVA structure. Hence, the C=C $\pi$ groups became C–C $\sigma$ groups. The C–H symmetric vibrational band at 2848 $cm^{-1}$ shifted to a higher wavenumber (nearly 2855 $cm^{-1}$) upon the addition of the $Bi^{3+}$ and $Tb^{3+}$ ions and f-MWCNTs. The absorption of the hydrogen ions from the free OH groups plays a pivotal role in the formation of the complexes. Moreover, it was clearly observed that the OH stretching vibrational band at 3670–3000 $cm^{-1}$ exhibited a decreased pattern with the incorporation of the dopant ions and f-MWCNTs, and also it shifted to a higher wavenumber. This encouraging result suggested the formation of non-covalent bonds between $Bi^{3+}$, $Tb^{3+}$ and the OH groups of the PVA skeleton.[20] From the FTIR spectra of the f-MWCNTs dispersed co-doped PVA:$Bi^{3+}$ + $Tb^{3+}$ polymer nanocomposite, the polymer complex formed probably *via* weak physical forces rather than strong chemical bonding forces with the nanoparticle environment. We observed the decreased transmittance in the FTIR spectra with the addition of the dopant ions and f-MWCNTs; this might be due to the complex formation and the presence of the f-MWCNTs within the polymer matrix.[21] Nevertheless, the significant bands of the f-MWCNTs, such as 1072 $cm^{-1}$, 1167 $cm^{-1}$, 1398 $cm^{-1}$ and 1733 $cm^{-1}$, are attributed to the stretching vibrations of C–O in the ether group, stretching vibrations of C–O in alcohol, O–H bending mode in the COOH group and the C=O in the COOH group, respectively. These pertinent bands regarding the f-MWCNTs are overlapping in the PVA complexed signals.[22] The decrease in the FTIR peak intensity in the FTIR spectral profile supports the complex formation between the dopant ions and the PVA polymer matrix, which is in good agreement with the XRD analysis.

### 4.4 Thermal analysis

The variation in the thermal properties of the prepared polymer matrices were systematically analyzed by TG/DTA profiles. Thermograms were recorded for (a) pure PVA, (b) PVA:$Bi^{3+}$, (c) PVA:$Tb^{3+}$, (d) PVA:($Bi^{3+}$ + $Tb^{3+}$), (e) PVA:($Bi^{3+}$ + $Tb^{3+}$) + f-MWCNTs (0.05 mg) polymer films in the temperature range from 25 °C to 700 °C, as shown in Fig. 4. The weight losses observed for each step along with the corresponding temperature for all the samples is given in Table 2. The decomposition of pure PVA occurs in three steps. The initial weight loss (around 7%) at 95 °C may be due to degradation of the large polymer chains into smaller fragments through primary decomposition and the removal of absorbed water could be because PVA is a hydrophilic polymer.[23] The second decomposition occurs at 289 °C with a weight loss of 68%, which is due to decomposition of the acetate and side-chains of PVA. The third decomposition occurs at 420 °C with a weight loss of 17%. This third degradation of the polymer is due to oxidation combustion of the PVA polymer main chain. The complete decomposition of pure PVA polymer is at 465 °C.[24] In the case of $Bi^{3+}$ and $Tb^{3+}$ doped and co-doped PVA polymer films with and without f-MWCNT, the first weight loss was at 94 °C, 89 °C, 84 °C and 91 °C with weight losses of 6%, 7%, 8% and 4% for (b) PVA:$Bi^{3+}$,

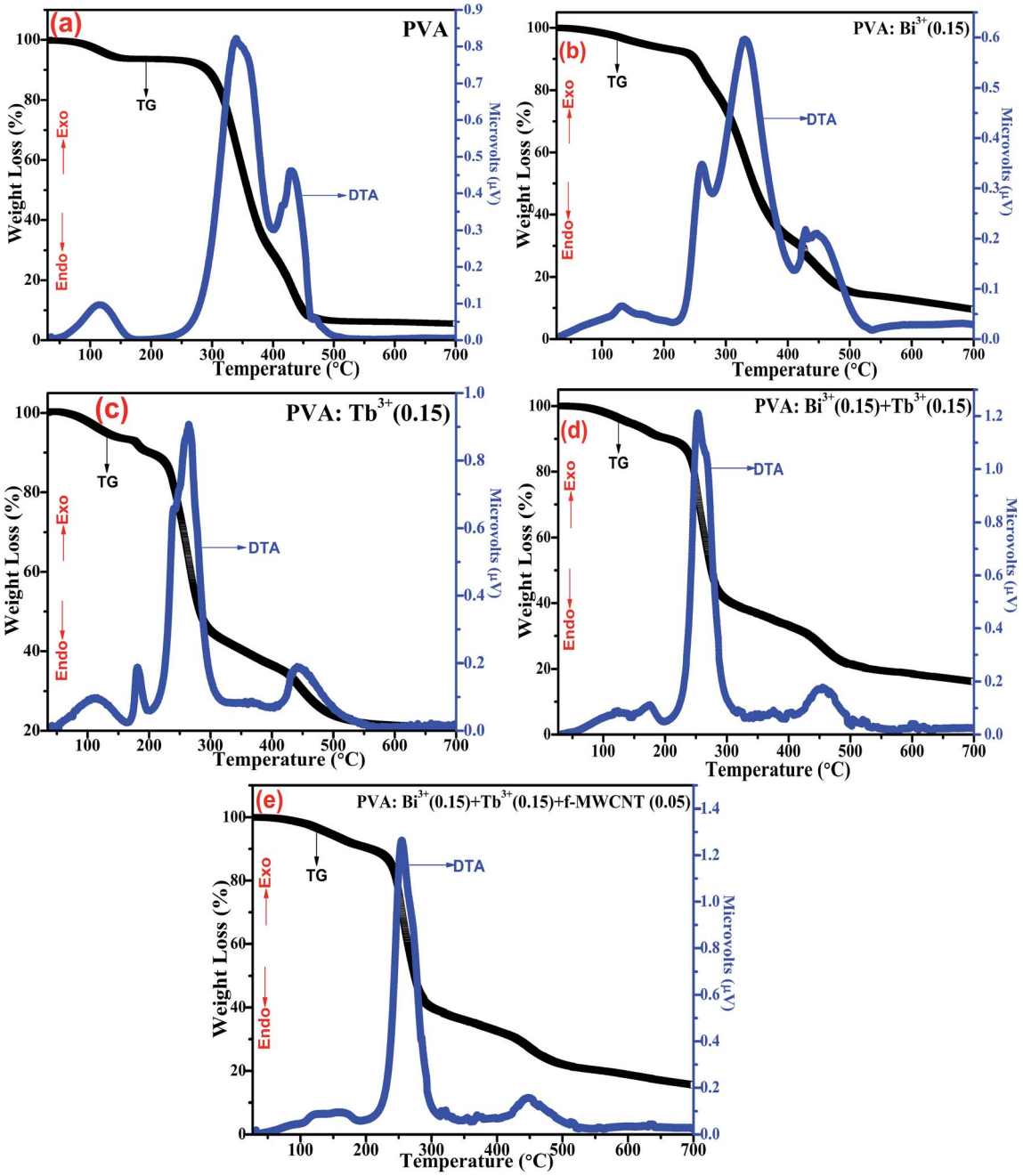


Fig. 4 TG/DTA profiles of (a) PVA, (b) $Bi^{3+}$:PVA, (c) $Tb^{3+}$:PVA, (d) ($Bi^{3+}$ + $Tb^{3+}$):PVA, (e) ($Bi^{3+}$ + $Tb^{3+}$) + f-MWCNTs (0.05 mg):PVA nanocomposite films.

(c) PVA:$Tb^{3+}$, (d) PVA:($Bi^{3+}$ + $Tb^{3+}$), (e) PVA:($Bi^{3+}$ + $Tb^{3+}$) + f-MWCNTs (0.05 mg):polymer films, respectively. This could be due to volatilization of small molecules or evaporation of the absorbed water from the polymer composites. This could result from micro-Brownian motion of the main chain back bone of the PVA polymer matrix. A small percentage of the weight loss occurred in doped samples at 168 °C, 178 °C, 182 °C and 178 °C with a weight loss of 5%, 4%, 4% and 6%, respectively. This lower value of weight loss suggests a phase transition that indicates the existence of a physical transition upon the addition of dopant ions. The third degradation temperature point was noticed in all the doped samples at 245 °C, 229 °C, 232 °C and 233 °C with weight losses of 47%, 45%, 44% and 42% for (b) PVA:$Bi^{3+}$, (c) PVA:$Tb^{3+}$, (d) PVA:($Bi^{3+}$ + $Tb^{3+}$), (e) PVA:($Bi^{3+}$ + $Tb^{3+}$) + f-MWCNTs (0.05 mg) polymer films, respectively. This thermal degradation occurred due to heating rearrangement of the polyene structure to the polyaromatic form. The decomposition of polyenes results in the formation of macroradicals, which further decompose to form *cis* and *trans* derivatives. Later on, they can form polyconjugated aromatic structures as a result of intramolecular cyclization and condensation reactions according to the Diels–Alder mechanism. The final step of the

 

Table 2 TG/DTA results for (a) PVA, (b) PVA:$Bi^{3+}$ (0.15), (c) PVA:$Tb^{3+}$ (0.15), (d) PVA:[$Bi^{3+}$ (0.15) + $Tb^{3+}$ (0.15)], (e) PVA:[$Bi^{3+}$ (0.15) + $Tb^{3+}$ (0.15) + f-MWCNT (0.05 mg)] polymer films

| | TG (degradation temperature with weight loss) (°C) (%) ± 2 | | | | DTA | |
|---|---|---|---|---|---|---|
| Sample | I$^{st}$ | II$^{nd}$ | III$^{rd}$ | IV$^{th}$ | $T_g$ (°C) | $T_m$ (°C) |
| (a) | 95 (7%) | — | 289 (68%) | 420 (17%) | 113 | 339 |
| (b) | 94 (6%) | 168 (5%) | 245 (47%) | 430 (14%) | 129 | 332 |
| (c) | 89 (7%) | 178 (4%) | 229 (45%) | 432 (10%) | 111 | 264 |
| (d) | 84 (8%) | 182 (4%) | 232 (44%) | 431 (10%) | 119 | 253 |
| (e) | 91 (4%) | 178 (6%) | 233 (42%) | 433 (9%) | 121 | 255 |

degradation was observed in all the doped samples above 440 °C, and it was due to thermo-oxidation of the carbonized residue.[25] All the thermal degradation was substantiated by the endothermic and exothermic peaks of the DTA profiles of all the polymer samples. The glass transition and melting temperatures were determined from the DTA profiles of the polymer composites, and these values are reported in Table 2. The $T_g$ values of the rare earth doped PVA polymer samples have a slight variation and a noteworthy variation in the f-MWCNTs embedded dual rare earth ion doped PVA polymer nanocomposite. This variation in the thermal properties is mainly due to the changes in the polymer interaction with respect to the hydrogen bonding and covalent bonding with the dopant ions, nanofiller dispersion, load transfer from the polymer molecules to the fillers, the crystallinity of the polymer matrix as well as the molecular packing of the polymer matrix. Among these, the polymer interactions between the polymer molecules and dopant salts or nanofillers were the most important because numerous other parameters such as crystallinity, molecular packing and degree of dispersion of nanofillers also depend on the interactions.[26] The thermal stability and melting temperatures of the rare earth ion doped PVA polymer composites and polymer nanocomposites decreased compared to pure PVA, and this might be due to a reduction in the number of intra and inter hydrogen bonds of PVA after the doping or dispersion of nanofiller. This is presumably due to the decrease in the degree of crystallinity as shown by XRD in earlier.[27]

### 4.5 Photoluminescence analysis

The photoluminescence excitation and emission spectral profiles of PVA:$Bi^{3+}$ polymer film are shown in Fig. 5. The outer $nS^2$ configuration in $Bi^{3+}$ is of great importance in the field of luminescence. The $Bi^{3+}$ ion has been widely used as a luminescence sensitizer in various rare earth doped complexes such as phosphors, glasses and polymer complexes.[28] $Bi^{3+}$ possesses a $6S^2$ electronic configuration, and its photoluminescence properties are dependent on the host composition. The ground state of $Bi^{3+}$ is $^1S_0$, and it consists of four excited states of $^3P_0$, $^3P_1$, $^3P_2$ and $^1P_1$ in increasing energy according to the electronic configuration of $Bi^{3+}$. However, the transitions of $^1S_0 \rightarrow {}^3P_0$ and $^1S_0 \rightarrow {}^3P_2$ are completely spin forbidden since the two levels of $^3P_1$ and $^1P_1$ are mixed by spin–orbit coupling. The spin selection

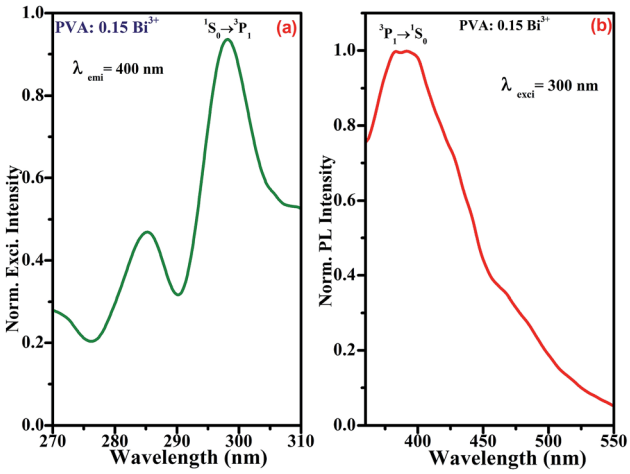


Fig. 5 (a) Excitation and (b) emission spectra of $Bi^{3+}$ (0.15 wt%):PVA polymer film.

rule in the $Bi^{3+}$ ion is considerably relaxed by the strong spin–orbit coupling. Hence, the transitions of $^1S_0 \rightarrow {}^3P_1$ and $^1S_0 \rightarrow {}^1P_1$ are expected to have reasonable absorption strengths. In the case of $Bi^{3+}$ doped samples, the absorption and emissions bands are attributed to the transitions of $^3P_1 \rightarrow {}^1S_0$ and $^1S_0 \rightarrow {}^3P_1$, respectively.[29] In our present case, the major excitation band is noticed at 300 nm apart from the other two low intensity bands at 385 nm and 370 nm in the PVA:$Bi^{3+}$ polymer complex, as shown in Fig. 5(a), and this excitation band is assigned to the corresponding electronic transition of $^1S_0 \rightarrow {}^3P_1$. Using this excitation, we can measure the emission spectrum, and the major emission is observed at 400 nm, as shown in Fig. 5(b). This emission band is assigned to the corresponding electronic transition of $^3P_1 \rightarrow {}^1S_0$.[30]

Fig. 6 shows the excitation spectrum of the PVA:$Tb^{3+}$ polymer composite film. Several excitation bands are observed in the excitation spectrum at 327 nm, 340 nm, 353 nm, 370 nm, 379 nm and 489 nm, and these bands are assigned to the

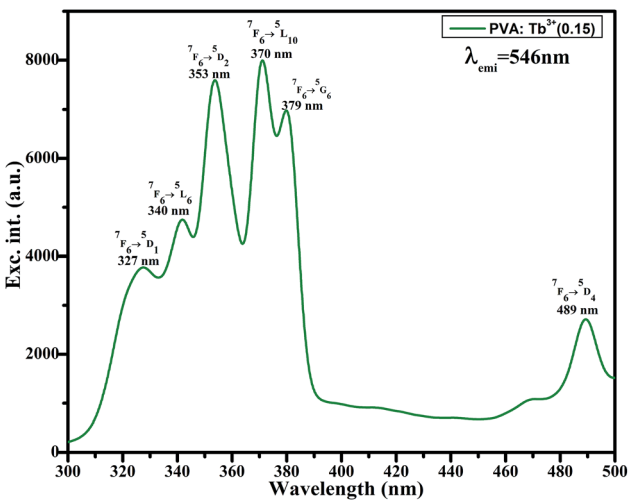


Fig. 6 Excitation spectrum of $Tb^{3+}$ (0.15 wt%):PVA polymer film.

corresponding electronic transitions as $^7F_6 \rightarrow {}^5D_1$, $^7F_6 \rightarrow {}^5L_6$, $^7F_6 \rightarrow {}^5D_2$, $^7F_6 \rightarrow {}^5L_{10}$, $^7F_6 \rightarrow {}^5G_6$ and $^7F_6 \rightarrow {}^5D_4$, respectively.[31] We observed the prominent excitation band at 370 nm ($^7F_6 \rightarrow {}^5L_{10}$) compared to the other excitation bands. The emission spectra of the PVA:$Tb^{3+}$ polymer composite films at different concentrations of $Tb^{3+}$ ions were studied using 370 nm ($^7F_6 \rightarrow {}^5L_{10}$) as the excitation wavelength, which is shown in Fig. 7. There were four emission bands observed in the emission spectra centered at 491 nm, 546 nm, 586 nm and 621 nm. These emission bands were assigned to the corresponding electronic transitions as ($^5D_4 \rightarrow {}^7F_6$), ($^5D_4 \rightarrow {}^7F_5$), ($^5D_4 \rightarrow {}^7F_4$) and ($^5D_4 \rightarrow {}^7F_3$), respectively.[32] The prominent green emission was observed from the PVA:$Tb^{3+}$ polymer composite films at 546 nm ($^5D_4 \rightarrow {}^7F_5$). Among the various concentrations of $Tb^{3+}$ ion doped PVA polymer composites, the 0.15 wt% concentration of the PVA:$Tb^{3+}$ polymer displayed a predominant emission intensity. Hence, the 0.15 wt% concentration of the $Tb^{3+}$ ions was the optimized concentration for better green emission. In order to enhance the fluorescence performance of the $Tb^{3+}$ (0.15 wt%):PVA polymer composite, we introduced a second suitable sensitizer ion, such as $Bi^{3+}$ ion, in different concentrations. Different concentrations (0.01, 0.02, 0.03, 0.04, 0.05, 0.075, 0.1, 0.15, 0.175, 0.2, 0.25 and 0.275 wt%) of $Bi^{3+}$ ions were added to the $Tb^{3+}$ (0.15 wt%):PVA polymer matrix for the preparation of co-doped samples for further investigation.

Both the excitation spectra of the $Tb^{3+}$ singly doped and co-doped PVA:$Tb^{3+}$ + $Bi^{3+}$ polymer composite films from monitoring the emission wavelength at 546 nm are shown in Fig. 8. The prominent excitation band is observed at 320 nm in the co-doped PVA:$Tb^{3+}$ + $Bi^{3+}$ polymer composite film. This indicates the presence of $Bi^{3+}$ ions along with $Tb^{3+}$ ions in the PVA polymer matrix. A slight difference was noticed between the excitation spectra with respect to the intensity and broadening of the spectral peaks. Apart from the existence of the same excitation bands of the $Tb^{3+}$ ion in the co-doped sample, the excitation peak intensity at 320 nm was enhanced, and a slight

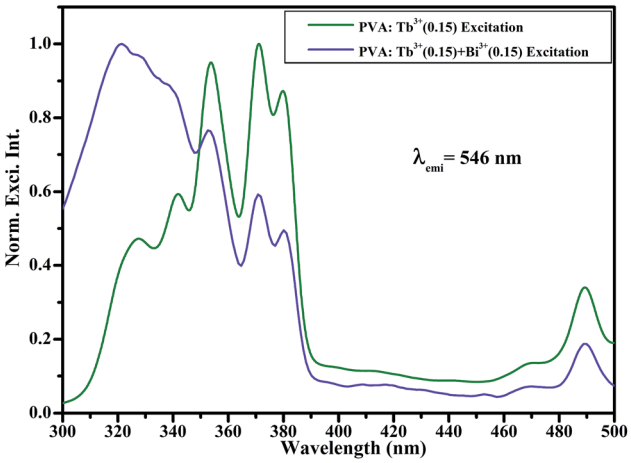


Fig. 8 Excitation spectra of $Tb^{3+}$ (0.15 wt%):PVA and $Bi^{3+}$ (0.15 wt%) + $Tb^{3+}$ (0.15 wt%):PVA polymer films.

broadening of the spectral peaks was observed in the co-doped PVA polymer system compared to the singly doped system. Other excitation band intensities pertaining to the $Tb^{3+}$ ions decreased. Therefore, it could be understood that their absorption and emission intensity were enhanced near the UV source. This favourable situation also strongly suggested the presence of $Bi^{3+}$ ions along with $Tb^{3+}$ ions and possible energy transfers were taking place from the $Bi^{3+}$ ions to the $Tb^{3+}$ ions in the co-doped PVA:$Tb^{3+}$ + $Bi^{3+}$ polymer matrix.[33] Using this 320 nm excitation, we obtained the photoluminescence spectra of PVA:$Tb^{3+}$ (0.15 wt%) + $Bi^{3+}$ polymer composite films by varying the $Bi^{3+}$ ion concentration, as shown in Fig. 9. Interestingly, we observed the significant emission properties in the co-doped PVA polymer matrix compared to the $Tb^{3+}$ singly doped PVA polymer system. The emission intensities were appreciably enhanced with the addition of $Bi^{3+}$ ions in different concentrations, as shown in Fig. 9. It is clearly shown that the green emission intensity of the $^5D_4 \rightarrow {}^7F_5$ transition becomes

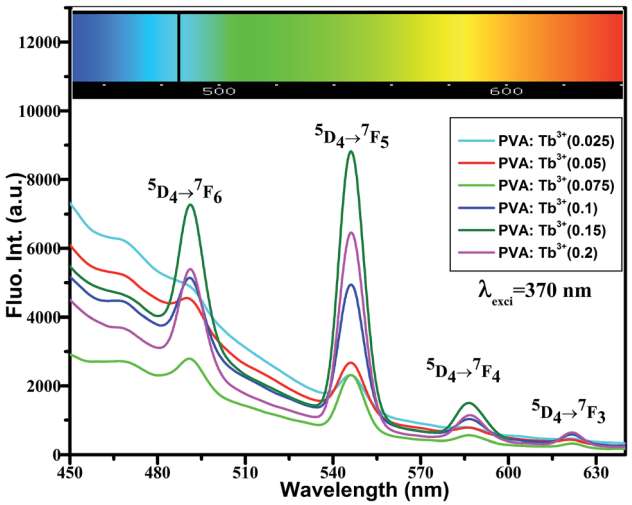


Fig. 7 Emission spectra of $Tb^{3+}$ (0.025, 0.05, 0.075, 0.1, 0.15 and 0.2 wt%):PVA polymer films.

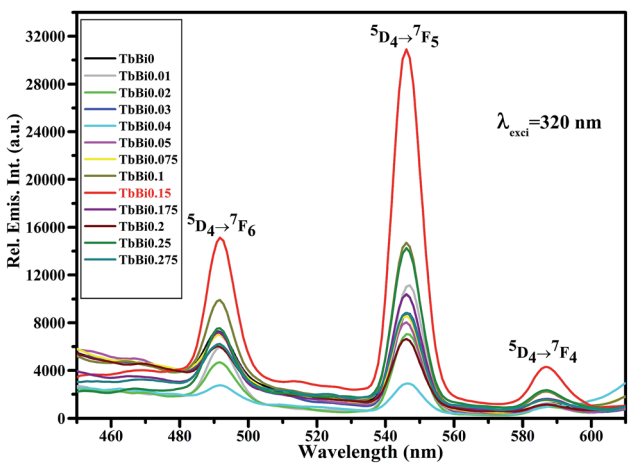


Fig. 9 Emission spectra of co-doped $Tb^{3+}$ (0.15 wt%) + $Bi^{3+}$ (0.01, 0.02, 0.03, 0.04, 0.05, 0.075, 0.1, 0.15, 0.175, 0.2, 0.25 and 0.275 wt%):PVA polymer films.

very strong in the co-doped system than the single $Tb^{3+}$ doped PVA polymer matrix. This could be due to possible energy transfer from the $Bi^{3+}$ ions to the $Tb^{3+}$ ions in the co-doped PVA polymer system.[34] Herein, $Bi^{3+}$ ions act as a sensitizer, and $Tb^{3+}$ ions act as an activator. Among all the concentrations of $Bi^{3+}$ ions, 0.15 wt% concentration of the $Bi^{3+}$ ion doped $Tb^{3+}$ (0.15 wt%):PVA polymer system exhibits predominant emission features over the others. Hence, we found that the optimized concentration of the sensitizer of $Bi^{3+}$ was 0.15 wt% based on the photoluminescence spectral features of the co-doped PVA polymer matrix. The emission intensities of the co-doped polymer matrix slowly decreased with the increasing $Bi^{3+}$ ion concentrations above 0.15 wt%. This might be due to the concentration quenching effect, which probably occurred as a result of an energy transfer due to more $Bi^{3+}$–$Bi^{3+}$ interactions than $Bi^{3+}$–$Tb^{3+}$.[35] All the above results demonstrate that $Bi^{3+}$ co-doping plays a pivotal role in improving the luminescence properties of $Tb^{3+}$ in the co-doped PVA polymer matrix. In this phenomenon, successful emission photons of $Bi^{3+}$ ions are collectively absorbed by the $Tb^{3+}$ ions within the PVA polymer matrix through energy transfer.

Another strategy to confirm the energy transfer phenomenon is the study of overlapped spectra of excitation and emission spectral profiles of the activator and sensitizer ions, respectively. This energy transfer takes place mainly due to radiative energy transfer through the emission of sensitizer ions and re-absorption by activator ions or the non-radiative condition between both of them. Herein, the principle condition for the energy transfer phenomenon is that the emission spectrum of the sensitizer should overlap with the excitation spectrum of the activator. The non-radiative energy transfer is accompanied by the electric multipole interactions and exchange interactions. The possible energy transfer probability is proportional to the energy overlap between the emission of the sensitizer and excitation of the activator. The energy overlap plays a pivotal role in the energy transfer phenomena.[36] The overlapped spectral profile of the emission of $Bi^{3+}$ and excitation spectrum of the $Tb^{3+}$ ion is shown in Fig. 10. We observed the well overlapped spectral region between the emission spectrum of $Bi^{3+}$ and the excitation spectrum of $Tb^{3+}$. Hence, this overlapped spectral profile satisfies the condition for an energy transfer between the $Bi^{3+}$ and $Tb^{3+}$ ions. This encouraging result suggested that the possible energy transfer was taking place between the $Bi^{3+}$ and $Tb^{3+}$ ions, and this is the only reason for the significant enhancement of the $Tb^{3+}$ ion emission intensities in the co-doped system. The schematic energy level for the energy transfer mechanism from $Bi^{3+}$ to $Tb^{3+}$ in the PVA polymer matrix is shown in Fig. 11.

In order to obtain further improvement in the photoluminescence properties of the co-doped PVA:($Bi^{3+}$ + $Tb^{3+}$) polymer films, several approaches for obtaining the prominent photoluminescence properties have been made. In another part of the energy transfer, f-MWCNTs were used to incorporate into the PVA:($Bi^{3+}$ + $Tb^{3+}$) PVA polymer matrix. Fig. 12(a) and (b) shows the fluorescence excitation and emission spectra of pure f-MWCNTs. From earlier reports, we realized that no emission was observed from the nonfunctionalized MWCNTs due to their

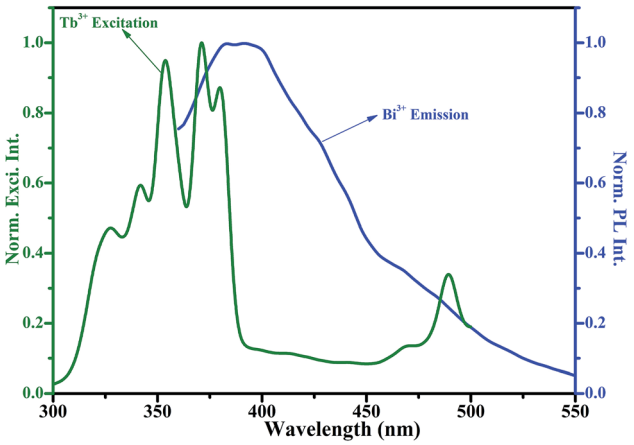


Fig. 10 Overlapped emission spectrum of $Bi^{3+}$ and excitation spectrum of $Tb^{3+}$:PVA polymer films.

metallic nature.[37] There are some reports on the photoluminescence properties of MWCNTs after functionalization.[38] Herein, we observed the major excitation band at 300 nm. The prominent emission was observed at 472 nm under the excitation of 300 nm in the pure f-MWCNTs. This emission could be attributed to the presence of defects at the nanotube surface after functionalization.[39]

**4.5.1. Energy transfer from $Bi^{3+}$ and f-MWCNTs to $Tb^{3+}$ ions simultaneously in co-doped PVA polymer composites.** There are no reports on the energy transfer based on the photoluminescence properties of f-MWCNT impregnated PVA:$Tb^{3+}$ polymer matrices as of now. We attempted to use f-MWCNTs to enhance the luminescence efficiency of the $Tb^{3+}$ ions in the PVA polymer matrix. The remarkable green emission was observed from the co-doped PVA:($Bi^{3+}$ + $Tb^{3+}$) composites under the excitation of 320 nm, as shown in Fig. 13. Surprisingly, the remarkable green emission enhancement was observed in the f-

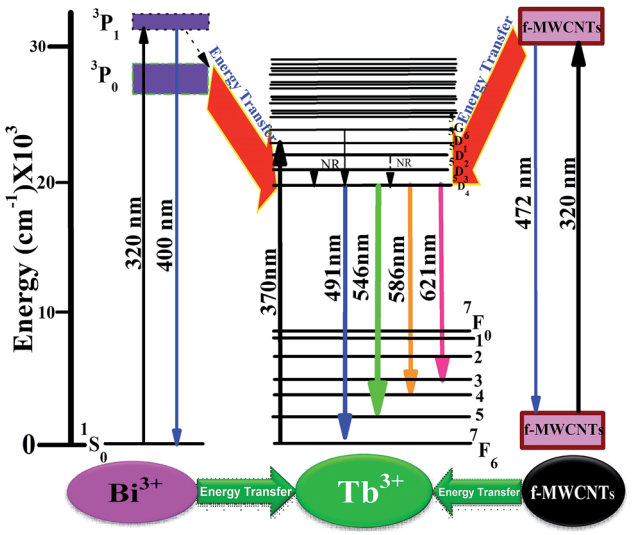


Fig. 11 Partial energy level scheme diagram of energy transfer from $Bi^{3+}$ to $Tb^{3+}$ and f-MWCNTs to $Tb^{3+}$in PVA polymer composite films.

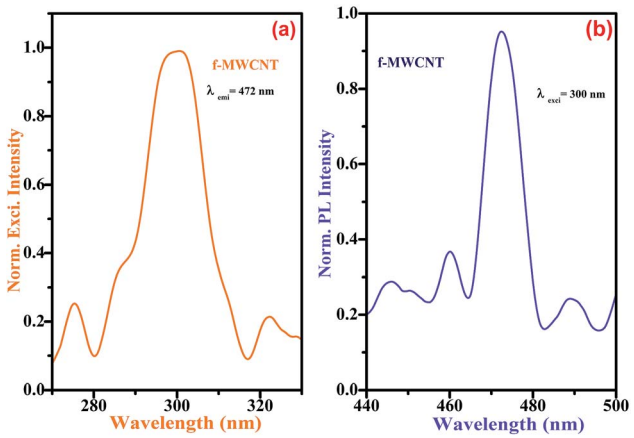


Fig. 12 (a) Excitation and (b) emission spectra of f-MWCNTs.

MWCNTs impregnated co-doped PVA:($Bi^{3+}$ + $Tb^{3+}$) polymer nanocomposites rather than the f-MWCNTs-free samples under 320 nm, as shown in Fig. 13. This encouraging result could be responsible for the energy transfer from the f-MWCNTs to the $Tb^{3+}$ ions, which increased the population of the excited $Tb^{3+}$ ions, or there might be an increase in the lifetime of the emitting energy level $^5D_4$ corresponding to $Tb^{3+}$ due to the interaction with f-MWCNTs. Upon increasing the f-MWCNTs concentration in the co-doped system, the emission intensities were enhanced, and a prominent emission was observed with 0.05 mg of f-MWCNTs impregnated in the co-doped PVA polymer nanocomposite. Hence, the optimized concentration of the f-MWCNTs was 0.05 mg. The reason for the enhancement in the $Tb^{3+}$ emission intensity with the addition of f-MWCNTs was that the possible energy transfer occurred from f-MWCNTs to $Tb^{3+}$. Defects like oxygen vacancies generally act as radiative centers in complexes. Essentially, the absorption cross-section band for the f-MWCNTs is very large, and numerous f-MWCNTs domains are excited from lower to higher energy states under UV

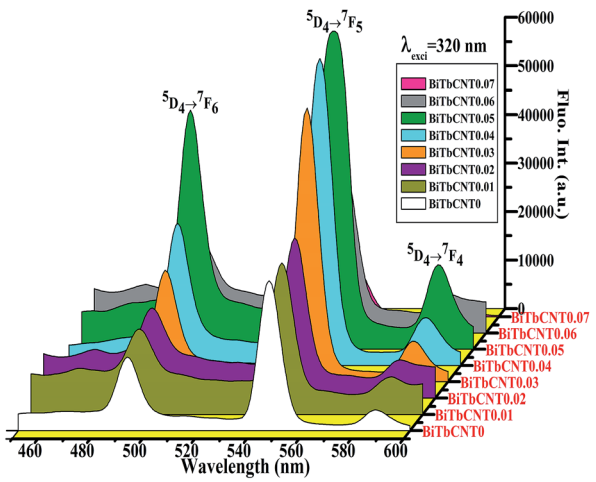


Fig. 13 Emission spectra of co-doped f-MWCNTs (0.01, 0.02, 0.03, 0.04, 0.05, 0.06 and 0.07 mg) embedded $Bi^{3+}$ (0.15 wt%) + $Tb^{3+}$ (0.15 wt%):PVA polymer nanocomposite films.

excitation. Moreover, the tubular structures of the f-MWCNTs might possess good surface to volume ratios. Due to the presence of high surface to volume ratios, the defects will also be ultimately enhanced. The surface defects and tubular morphology altogether could produce more luminescence centers, which acted as sensitizer portions to enhance the $Tb^{3+}$ emission intensity.[40] The result of the $^5D_4$ level would naturally enhance the intensity of all the $^5D_4 \rightarrow {}^7F_J$ ($J = 0$–6) transitions with increasing $Tb^{3+}$ ions. The relative increase in the intensities of the different bands will depend on the intrinsic probabilities for the individual transitions. However, the largest increase in intensity is found for the transition $^5D_4 \rightarrow {}^7F_5$, which is a magnetic dipole allowed hypersensitive transition. This hypersensitive nature is most responsible for the large increase in the intensity seen in the presence of f-MWCNTs. From the above discussion, we concluded that the possible energy transfer takes place from $Bi^{3+}$ to $Tb^{3+}$ and f-MWCNTs to $Tb^{3+}$ unambiguously. The superposition integral of the spectral shapes between the donor (f-MWCNTs) emission and acceptor ($Tb^{3+}$) excitation is proportional to the energy transfer probability.[41] We observed the overlapped spectral region between the emission spectrum of the f-MWCNTs and excitation spectrum of $Tb^{3+}$, as shown in Fig. 14(a). Moreover, there are no overlapped spectral regions between $Bi^{3+}$ excitation and f-MWCNTs emission, which suggests that the energy transfer might not take place from the f-MWCNTs to $Bi^{3+}$, as shown in Fig. 14(b). From this discussion, we suggest that the energy transfer took place from $Bi^{3+}$ to $Tb^{3+}$ and f-MWCNTs to $Tb^{3+}$ under 320 nm of excitation.

CIE chromaticity diagram pertaining to PVA:$Tb^{3+}$ (0.15), PVA:$Bi^{3+}$ (0.15) + $Tb^{3+}$ (0.15) and PVA:$Bi^{3+}$ (0.15) + $Tb^{3+}$ (0.15) + f-MWCNTs (0.05 mg) polymer composites is shown in Fig. 15. We observed low violet-green and light green emissions in the singly doped and co-doped PVA:$Tb^{3+}$ (0.15) and PVA:$Bi^{3+}$ (0.15) + $Tb^{3+}$ (0.15) polymer composites, respectively. A certain increment was noticed in the color index in the co-doped PVA:$Bi^{3+}$ (0.15) + $Tb^{3+}$ (0.15) sample compared to the singly doped PVA:$Tb^{3+}$ (0.15) polymer composite. CIE chromaticity coordinates ($x$ and $y$) for (i) PVA:$Tb^{3+}$ (0.15), (ii) co-doped PVA:$Bi^{3+}$ (0.15) + $Tb^{3+}$ (0.15) and (iii) f-MWCNTs (0.05 mg) impregnated co-doped PVA:$Bi^{3+}$ (0.15) + $Tb^{3+}$ (0.15) polymer nanocomposites are presented in Table 3. By dispersion of the f-MWCNTs at a 0.05 mg concentration, the chromaticity coordinates could be turned to the green position under 320 nm. This could be external evidence for the energy transfer process from the f-MWCNTs to the $Tb^{3+}$ ions in the PVA polymer matrix.

### 4.6 Decay analysis

Another strategy to confirm the energy transfer phenomena is lifetime decay analysis. The decay curve profiles pertaining to singly doped $Tb^{3+}$ ions and co-doped PVA polymer composites have been extensively studied and are shown in Fig. 16. In the case of singly doped $Tb^{3+}$:PVA polymer system, the luminescence (green emission at 546 nm) lifetime for the $^5D_4$ excited states of the $Tb^{3+}$ ion with an excitation of 370 nm was calculated, and it was found to be 0.451 ms. However, we observed

 

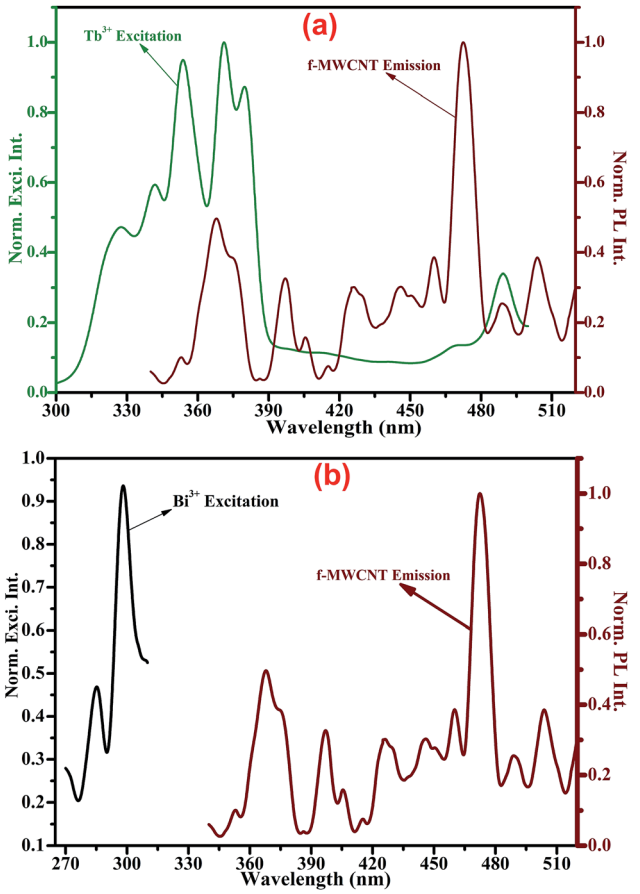


Fig. 14 Overlapped spectral profiles of (a) emission spectrum of synthesized f-MWCNTs and excitation spectrum of $Tb^{3+}$:PVA polymer film and (b) emission spectrum of synthesized f-MWCNTs and excitation spectrum of $Bi^{3+}$:PVA polymer film.

the decay curve of the singly doped $Tb^{3+}$:PVA polymer system that fitted well in the single exponential function, as shown in Fig. 16. It can be seen that the lifetime decay curve is well fitted to follow a single exponential decay. The lifetime is calculated by fitting the curve to the following equation:

$$I_t = I_0 \exp(-t/\tau) \quad (1)$$

where $I_t$ and $I_0$ are the intensities at time $t$ and 0, respectively, and $\tau$ refers to the luminescent lifetime. In the co-doped system, the decay curves exhibit non-exponential behavior due to the different sites of the $Tb^{3+}$ ions. However, the lifetime decay curve is fitted by the expression given as

$$I(t) = A_1 \exp(-t/\tau_1) + A_2 \exp(-t/\tau_2) \quad (2)$$

where $I(t)$ is the emission intensity, $A_1$ and $A_2$ are constants, $\tau_1$ and $\tau_2$ are the short and long lifetimes, respectively. The average lifetimes ($\tau_{avg}$) of the $Tb^{3+}$ ions were determined by the formula:

$$\tau_{avg} = \frac{A_1\tau_1^2 + A_2\tau_2^2}{A_1\tau_1 + A_2\tau_2} \quad (3)$$

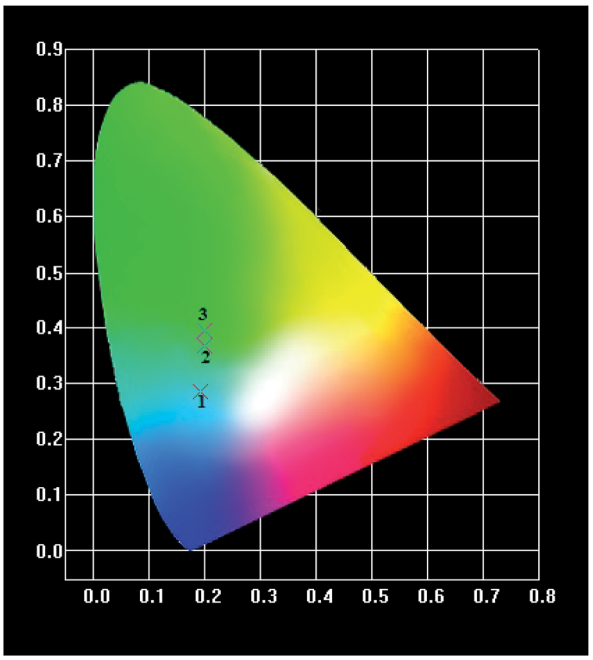


Fig. 15 CIE chromaticity diagram for $Tb^{3+}$ (0.15 wt%):PVA, co-doped $Bi^{3+}$ (0.15 wt%) + $Tb^{3+}$ (0.15 wt%):PVA, f-MWCNTs (0.05 mg) embedded co-doped $Bi^{3+}$ (0.15 wt%) + $Tb^{3+}$ (0.15 wt%):PVA polymer nanocomposites.

However, the $Tb^{3+}$ co-doped PVA polymer film decay curves slightly deviated from the single exponential nature compared with the decay curve of the singly doped PVA polymer composite. This could be due to the modification of the fluorescent dynamics by the co-doped ions. The non-exponential nature of the decay curve regarding the co-doped system was observed. This favorable existence of the non-exponential nature of the decay profile indicated the interaction between the acceptor and donor ions. The availability of the donor ($Bi^{3+}$) ions per acceptor ($Tb^{3+}$) ion will be more in the co-doped polymer composite; therefore, the average distance between the acceptor–donor ions decreased, which led to electronic multipole–multipole interactions. This condition is preferable for energy transfer. Consequently, the abovementioned lifetime decay dynamics strongly suggested that the efficient energy transfer process takes place from $Bi^{3+}$ to $Tb^{3+}$ in the PVA polymer film.[42]

By co-doping with $Bi^{3+}$ and $Tb^{3+}$, the $Tb^{3+}$ emission peak (546 nm) intensity was remarkably enhanced under the excitation at 320 nm, which is related to $Bi^{3+}$. Consequently, its lifetime was also considerably increased. The emission lifetime of the $Tb^{3+}$ in the co-doped polymer matrix was 0.803 ms. It can be observed that the lifetime of the $^5D_4$ levels of the $Tb^{3+}$ in the co-doped system increased more than the singly doped polymer system. The co-doped polymer lifetime decay curve of $Tb^{3+}$ ions with the excitation of 320 nm fit well to a non-exponential function, as shown in Fig. 16. This is confirmed that efficient energy migration has been taking place from the $Bi^{3+}$ to $Tb^{3+}$ in the PVA polymer composite.[43]

Table 3 CIE chromaticity coordinates of PVA:$Tb^{3+}$ (0.15), PVA:$Bi^{3+}$ (0.15) + $Tb^{3+}$ (0.15) and PVA:$Bi^{3+}$ (0.15) + $Tb^{3+}$ (0.15) + f-MWCNTs (0.05 mg) polymer composites under the common excitation of 320 nm

| Sl. no. | Sample composition (wt%) | CIE coordinates ($x$, $y$) |
|---|---|---|
| 1 | PVA:$Tb^{3+}$ (0.15) | (0.1924, 0.2842) |
| 2 | PVA:$Bi^{3+}$ (0.15) + $Tb^{3+}$ (0.15) | (0.1992, 0.3664) |
| 3 | PVA:$Bi^{3+}$ (0.15) + $Tb^{3+}$ (0.15) + f-MWCNT (0.015) | (0.1998, 0.3942) |

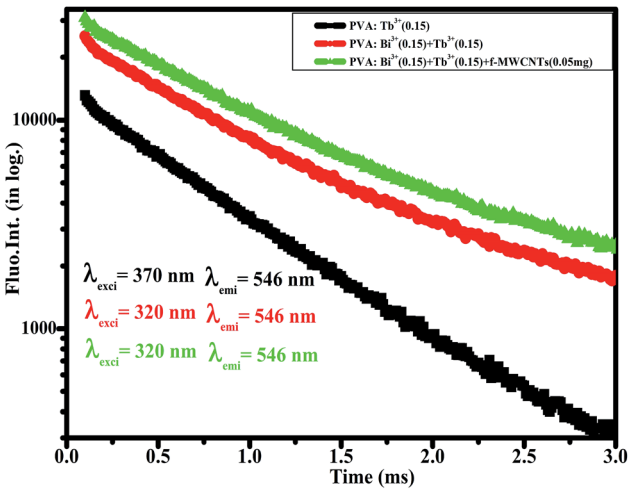


Fig. 16 Decay curves of $Tb^{3+}$ emissions in the single and co-doped PVA polymer matrix with and without f-MWCNTs.

Upon adding the f-MWCNTs (0.05 mg) to the co-doped ($Bi^{3+}$ + $Tb^{3+}$):PVA polymer system, the lifetime of the $^5D_4$ levels of the $Tb^{3+}$ ions increased. This could be due to the coupling effect of the plasmonic field of the nanoparticles and rare earth ions. This might influence the rare earth ion radiative level lifetime and energy migration. The f-MWCNTs were impregnated along with both $Bi^{3+}$ and $Tb^{3+}$ in the co-doped polymer composite, and the lifetime of the green emission regarding the $Tb^{3+}$ ions was 0.857 ms. The lifetime improvement by the addition of $Bi^{3+}$ and f-MWCNTs to the $Tb^{3+}$ doped PVA complex confirmed the existence of energy transfer from the $Bi^{3+}$ ions and f-MWCNTs to $Tb^{3+}$. The lifetime decay curve pertaining to the $Tb^{3+}$ ions in the f-MWCNTs impregnated co-doped PVA polymer matrix had a non-exponential nature, which supports the efficient interaction between the acceptor and donor ions.[44] The energy transfer mechanism was evidently interpreted by the schematic energy level diagram and is shown in Fig. 11.

## 5. Conclusion

We successfully prepared $Bi^{3+}$, $Tb^{3+}$ doped and co-doped PVA polymer composite films with and without functionalized multiwalled carbon nanotubes (f-MWCNTs) using a solution casting method. The XRD profiles revealed that the prepared PVA polymer composite films exhibit a semi-crystalline nature. FTIR spectral analysis confirmed the complex formation and ion–polymer interactions with the incorporation of both rare earth ions into the polymer composite along with the f-MWCNTs. The thermal stability and decomposition dynamics of the pure PVA, $Bi^{3+}$, $Tb^{3+}$ doped PVA polymer composite films with and without f-MWCNTs were evaluated by TG/DTA profiles. The optical properties were systematically analysed by optical absorption and luminescence spectral studies. Terbium doped PVA polymer composite films exhibited a *green* emission with a UV excitation source. The prominent green emission at 546 nm ($^5D_4 \rightarrow {}^7F_5$) of the $Tb^{3+}$ ions was observed, and other transitions of $Tb^{3+}$ were clearly explained. The optimized concentration of the $Tb^{3+}$ ions was 0.15 wt% in the singly doped $Tb^{3+}$:PVA polymer matrix. PL efficiency of $Tb^{3+}$ ions was increased by co-doping with $Bi^{3+}$ through the energy transfer process. The optimized sensitizing concentration of the $Bi^{3+}$ ions in the co-doped $Bi^{3+}$ + $Tb^{3+}$:PVA polymer system was 0.15 wt% based on the fluorescence spectral analysis of the co-doped polymer system. Surprisingly, the emission performances of the $Tb^{3+}$ ions in the co-doped polymer complex were remarkably enhanced by the addition of the f-MWCNTs to the co-doped $Bi^{3+}$ + $Tb^{3+}$:PVA polymer system. This could be due to efficient energy transfer taking place from the f-MWCNTs to the $Tb^{3+}$ ions. In the f-MWCNTs embedded $Bi^{3+}$ + $Tb^{3+}$:PVA polymer system, an energy migration between the f-MWCNTs and $Tb^{3+}$ ions took place in the PVA polymer. The sensitizing effect of the f-MWCNTs and $Bi^{3+}$ ions significantly improved the emission performance of the $Tb^{3+}$ ions. This dual way energy transfer phenomena were substantiated by several fluorescence methods. The energy migration pathway was clearly elucidated through partial energy level scheme diagrams and lifetime decay dynamics. These bright green luminescent polymer nanocomposite materials could be suggested as promising candidates for green luminescent photonic applications.

## Acknowledgements

This study was supported by the Basic Science Research Program through the National Research Foundation of Korea (NRF) funded by the Ministry of the Science ICT & Future Planning (NRF-2015R1A1A3A04001268).

## References

1 R. Decadt, K. Van Hecke, D. Depla, K. Leus, D. Weinberger, I. Van Driessche, P. Van Der Voort and R. Van Deun, *Inorg. Chem.*, 2012, **51**, 11623–11634.
2 Q. D. Ling, D. J. Liaw, C. Zhu, D. S. H. Chan, E. T. Kang and K. G. Neoh, *Prog. Polym. Sci.*, 2008, **33**, 917–978.
3 X. J. Sun, W. X. Li, W. J. Chai, T. Ren and X. Y. Shi, *J. Fluoresc.*, 2010, **20**, 453.
4 K. Binnemans, *Chem. Rev.*, 2009, **109**, 4283–4374.
5 M. Obula Reddy and B. Chandra Babu, *Indian Journal of Materials Science*, 2015, **2015**, 1–8.
6 J. Y. Park, H. C. Jung, G. Seeta Rama Raju, B. K. Moona, J. H. Jeong, S.-M. Son and J. H. Kim, *Mater. Res. Bull.*, 2010, **45**, 572–575.
7 A. M. Srivastava, *J. Lumin.*, 1996, **69**, 301–309.

8 T. Hasegawa, N. Sato, S. W. Kim, T. Ishigaki, K. Uematsu, K. Toda and M. Sato, *J. Ceram. Soc. Jpn.*, 2015, **123**(6), 507–511.
9 J. A. Jiménez, S. Lysenko and H. Liu, *J. Lumin.*, 2008, **128**, 831–833.
10 G. Kaur, R. K. Verma, D. K. Rai and S. B. Rai, *J. Lumin.*, 2012, **132**, 1683–1687.
11 X. Wang, S. Yang, W. Shi, J. Li, T. Hayat and X. Wang, *Environ. Sci. Technol.*, 2015, **49**, 11721–11728.
12 H.-X. Wu, W.-M. Cao, J. Wang, H. Yang and S.-P. Yang, *Nanotechnology*, 2008, **19**, 345701–345710.
13 G. Ovejero, J. L. Sotelo, M. D. Romero, A. Rodrıguez, M. A. Ocana, G. Rodrıguez and J. Garcıa, *Ind. Eng. Chem. Res.*, 2006, **45**, 2206–2212.
14 T. Zhao, C. Hou, H. Zhang, R. Zhu, S. She, J. Wang, T. Li, Z. Liu and B. Wei, *Sci. Rep.*, 2014, **5619**(4), 1–7.
15 C.-M. Tang, Yi-H. Tian and S.-H. Hsu, *Materials*, 2015, **8**, 4895–4911.
16 H. J. Salavagione, G. Martınez and M. A. Gomez, *J. Mater. Chem.*, 2009, **19**, 5027–5032.
17 E. Sheha, M. Nasr and M. K. El-Mansy, *Phys. Scr.*, 2013, **88**, 035701–035709.
18 X. Qi, X. Yao, S. Deng, T. Zhou and Q. Fu, *J. Mater. Chem. A*, 2014, **2**, 2240–2249.
19 S. Kayal and R. V. Ramanujan, *Mater. Sci. Eng., C*, 2010, **30**, 484–490.
20 T. A. Hamdalla and T. A. Hanafy, *Optik*, 2016, **127**, 878–882.
21 M. Z. Kassaee, M. Mohammadkhani, A. Akhavan and R. Mohammadi, *Struct. Chem.*, 2011, **22**, 11.
22 D. Lai, Y. Wei, L. Zou, Y. Xu and H. Lu, *Prog. Nat. Sci.: Mater. Int.*, 2015, **25**, 445–452.
23 K. Zhou, S. Jiang, C. Bao, L. Song, B. Wang, G. Tang, Y. Hu and Z. Gui, *RSC Adv.*, 2012, **2**, 11695–11703.
24 S. Ramesh and A. K. Arof, *J. Power Sources*, 2001, **99**, 41–47.
25 A. Y. Shaulov, S. M. Lomakin, T. S. Zarkhina, A. D. Rakhimkulov, N. G. Shilkina, Y. B. Muravlev and A. A. Berlin, *Dokl. Phys. Chem.*, 2005, **403**, 154–158.
26 S. K. Sharma, J. Prakash and P. K. Pujari, *Phys. Chem. Chem. Phys.*, 2015, **17**, 29201–29209.
27 Y. Pavani, M. Ravi, S. Bhavani, A. K. Sharma and V. V. R. NarasimhaRao, *Polym. Eng. Sci.*, 2012, **52**, 1685–1692.
28 W. Xu, M. Peng, Z. Ma, G. Dong and J. Qiu, *Opt. Express*, 2012, **20**(14), 15692–15702.
29 X. Y. Huang, X. H. Ji and Q. Y. Zhang, *J. Am. Ceram. Soc.*, 2011, **94**(3), 833–837.
30 L. J. Wang, H. Guo, Y. L. Wei, H. M. Noh and J. H. Jeong, *Opt. Mater.*, 2015, **42**, 233–236.
31 J. F. M. dos Santos, I. A. A. Terra, N. G. C. Astrath, F. B. Guimaraes, M. L. Baesso, L. O. A. Nunes and T. Catunda, *J. Appl. Phys.*, 2015, **117**, 053102.
32 C. R. Kesavulu, A. C. Almeida Silva, M. R. Dousti, N. O. Dantas, A. S. S. de Camargo and T. Catunda, *J. Lumin.*, 2015, **165**, 77–84.
33 V. Rao Bandi, B. K. Grandhe, K. Jang, D.-S. Shin, S.-S. Yi and J.-H. Jeong, *Mater. Chem. Phys.*, 2013, **140**, 453–457.
34 Y. Xia, Y. Huang, Q. Long, S. Liao, Y. Gao, J. Liang and J. Cai, *Ceram. Int.*, 2015, **41**, 5525–5530.
35 S. Yan, J. Zhang, X. Zhang, S. Lu, X. Ren, Z. Nie and X. Wang, *J. Phys. Chem. C*, 2007, **111**, 13256–13260.
36 Z. Nan-Fei, L. Yong-Xiang and Y. Xiao-Feng, *Chin. Phys. Lett.*, 2008, **25**(2), 703–706.
37 Y. V. Fedoseeva, L. G. Bulusheva, A. V. Okotrub, M. A. Kanygin, D. V. Gorodetskiy, I. P. Asanov, D. V. Vyalikh, A. P. Puzyr and V. S. Bondar, *Sci. Rep.*, 2015, **9379**(5), 1–7.
38 Y. Lin, B. Zhou, R. B. Martin, K. B. Henbest, B. A. Harruff, J. E. Riggs, Z.-X. Guo, L. F. Allard and Y.-P. Sun, *J. Phys. Chem. B*, 2005, **109**(31), 14779–14782.
39 D. K. Singh, P. K. Iyer and P. K. Giri, *NanoTrends*, 2008, **4**(1), 55–58.
40 B. K. Grandhe, V. R. Bandi, K. Jang, S. S. Kim, D.-S. Shin, Y. Lee, J.-M. Lim and T. Song, *Met. Mater. Int.*, 2013, **19**(3), 507–511.
41 M. Mattarelli, M. Montagna, L. Zampedri, A. Chiasera, M. Ferrari, G. C. Righini, L. M. Fortes, M. C. Goncalves, L. F. Santos and R. M. Almeida, *Europhys. Lett.*, 2005, **71**, 394.
42 Z. Zhu, G. Fu, Y. Yang, Z. Yang and P. Li, *J. Mater. Sci.*, 2016, **51**, 6944–6954.
43 D. Wen, J. Feng, J. Li, J. Shi, M. Wu and Q. Su, *J. Mater. Chem. C*, 2015, **3**, 2107–2114.
44 L. Zhou, P. A. Tanner, L. Ning, W. Zhou, H. Liang and L. Zheng, *J. Phys. Chem. A*, 2016, **120**(28), 5539–5548.